applied sciences

MDPI

Article

Experimental and Numerical Study of the Thermal Properties of Dry Green Swales to Be Used as Part of Geothermal Energy Systems

Carlos Rey-Mahía [1,*], Felipe P. Álvarez-Rabanal [2] and Luis Á. Sañudo-Fontaneda [1]

[1] Civil, Environmental and Geomatics Engineering Research Group (CEGE), Department of Construction and Manufacturing Engineering, Campus of Mieres, University of Oviedo, Gonzalo Gutiérrez Quirós s/n, 33600 Mieres, Spain; sanudoluis@uniovi.es

[2] Sustainable Construction, Simulation and Testing Research Group (GICONSIME), Department of Construction and Manufacturing Engineering, Campus of Mieres, University of Oviedo, Gonzalo Gutiérrez Quirós s/n, 33600 Mieres, Spain; alvarezfelipe@uniovi.es

* Correspondence: uo236881@uniovi.es; Tel.: +34-985-458-196

Featured Application: This study can be applied in order to design geothermal systems in combination with Sustainable Drainage Systems (SuDS), taking into account their thermal considerations.

Abstract: Low-enthalpy geothermal systems are a promising source for renewable and clean energy for heating, cooling, and air conditioning residential buildings, contributing to the reduction in greenhouse gas emissions in line with the United Nations' Sustainable Development Goals. Previous research emerged around the geothermal utilization of Sustainable Drainage Systems (SuDS) as multifunctional surfaces for stormwater control and energy saving, developing the water–energy nexus. However, these studies did not comprehensively considered the energy aspects for SuDS design, using non-standardized tests to measure the main thermal parameters. This research aims to address this gap by proposing a novel hybrid engineering procedure to study the thermal properties of SuDS layers and materials through experimental tests combined with steady-state and transient numerical simulations, using green swales operating under dry and wet conditions as a first case study for SuDS techniques. Novel materials incorporated into dry swales (expanded clay and construction and demolition waste) were tested. The results validated this new methodology, reporting an increase of 87% under dry conditions, and 51% under wet scenarios in the thermal insulation performance in comparison to standard materials. A better thermal performance of the systems can be achieved by approaching SuDS design from a holistic viewpoint that integrates energy aspects.

Keywords: construction and demolition waste (CDW); green infrastructure (GI); ground-source heat pumps (GSHP); hot-box test; low impact development (LID); modified transient plane source (MTPS); nature-based solutions (NBS); stormwater best management practices (BMPs); stormwater control measures (SCMs); Sustainable Drainage System (SuDS); water-sensitive urban design (WSUD); energy–water nexus

Citation: Rey-Mahía, C.; Álvarez-Rabanal, F.P.; Sañudo-Fontaneda, L.Á. Experimental and Numerical Study of the Thermal Properties of Dry Green Swales to Be Used as Part of Geothermal Energy Systems. *Appl. Sci.* **2023**, *13*, 10644. https://doi.org/10.3390/app131910644

Academic Editors: María Isabel Rodríguez Rojas and Montserrat Zamorano

Received: 28 August 2023
Revised: 18 September 2023
Accepted: 22 September 2023
Published: 25 September 2023

1. Introduction

Geothermal energy has established itself as a renewable and sustainable energy source with great potential in response to the growing demand for energy and the need to reduce greenhouse gas emissions [1]. A report by the Massachusetts Institute of Technology (MIT) concluded that geothermal energy has the potential to provide a highly efficient and sustainable energy source with the capacity to generate a significant amount of electricity worldwide [2]. This renewable energy source aligns with the United Nations' (UN) Sustainable Development Goals (SDGs), specifically SDG7, which "*aims to ensure access to affordable, reliable, sustainable and clean energy*" [3]. It is also aligned with the European Union's (EU)

energy objectives, aiming for climate neutrality by 2050 [4]. To achieve this goal, the EU has developed several directives and regulations to encourage the development and implementation of renewable energies, including geothermal energy [5]. In addition to these UN and EU initiatives, there are numerous countries across the globe that have promoted the use of geothermal energy. For instance, the U.S. Department of Energy is strongly supporting the development and deployment of low-enthalpy geothermal systems [6].

Shallow geothermal systems (SGS), also known as low-enthalpy geothermal systems [7] have been highlighted as a promising alternative for heating and cooling buildings, as well as for other industrial and agricultural applications [8]. Moreover, geothermal power generation can make up for the elevated energy demands of numerous industrial procedures reducing their costs [9]. Heating and cooling buildings using geothermal heat pumps is the most energy- and environmentally efficient system, and the most cost-effective from an economic standpoint [10]. It has been demonstrated that the cost of heating one square meter of space utilizing geothermal systems is less expensive than traditional energy sources [11]. The heat exchangers are located in transitional thermal domains, which are influenced by the atmospheric temperature in shallow horizontal geothermal systems [12]. Despite this scenario, they offer better performance than when functioning under atmospheric conditions throughout the year [13], given the fact that the further down they are placed into the ground, the more stable the temperatures are throughout the year [14]. This is a key factor in this type of system and it is important in order to minimize the influence of the ambient temperature on Geothermal Heat Exchangers (GHEs) [15].

Various authors have explored the implications and importance of the water–energy nexus within the need for further implementation of SGS [16]. Both water and energy are critical resources that future societies have to address [17], particularly given the influence of climate change and unpredictable scenarios. Previous investigations have paved the way for the study of the role of geothermal systems and their potential combination with Sustainable Drainage Systems (SuDS) with a special interest in the exploration of SGS [18]. SuDS are a set of drainage techniques, which, in many cases, are included under the nature-based solution (NBS) framework where they are designed with nature at their core. SuDS aim to address stormwater management at local and micro-scales in specific locations with particular weather and site constraints [19,20]. SuDS are guided by the urban design philosophy known as water-sensitive urban design (WSUD), which encompasses a wide range of techniques from SuDS to environmental techniques such as those described in low-impact development (LID) [21]. These techniques aim to restore the natural hydrological cycle while managing the quantity and quality of stormwater [22]. Simultaneously, they create new spaces that promote amenities and biodiversity in cities [23].

Permeable Pavement Systems (PPSs) [24], perhaps one of the most widespread SuDS techniques [25], were the main SuDS technique studied in previous investigations in the literature. The performance of an SGS combined with a PPS was simulated in laboratory experiments [26] but lacked a validation tool such as numerical modeling. The state of the art shows studies focusing on the hydraulic performance and pollutant mitigation capacity of these systems but leaving the thermal performance aside [27,28]. On the other hand, other studies conducted field experiments under real conditions, centering their efforts in the analysis of PPSs in combination with an SGS [18,24]. These studies helped in paving the way towards the understanding of how "grey" SuDS design can be improved to integrate SGS and energy conservation. However, they showed the need to further develop the so-called "green" SuDS (those with a vegetative base including in NBS) and their potential to house SGS. Following up from these initial steps in the scientific literature, vegetated swales were incorporated into the scientific narrative, outlining the viability of geothermal utilization in other SuDS with a higher ecosystem potential (see Figure 1) [29]. Swales are one of the most promising SuDS techniques due to its simplicity of design and versatility for implementation both in urban environments and transport infrastructures such as roads [30]. There are mainly three types of vegetated swales based on their geometry and hydraulic behavior: dry, wet, and conveyance and attenuation swales [31]. Among these

three typologies, the dry swale is considered the most suitable for the potential combination with SGS [29]. These type of swales, due to their geometry, are constructed at a greater depth, making them compatible with the minimum ones required for the installation of GHEs [32,33].

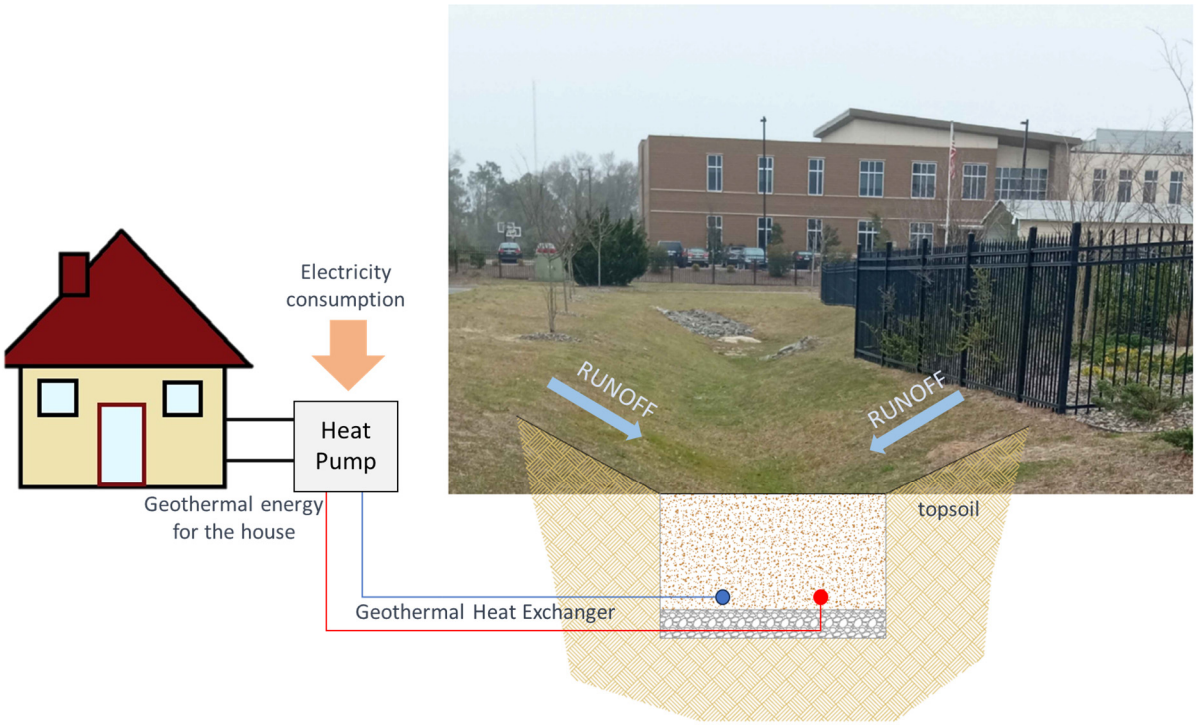

Figure 1. Schematic diagram of the proposed system outlined under a standard green swale.

Before designing a shallow geothermal installation, studying and determining the thermal properties of the materials beneath the point where the heat exchanger will be located is essential (see Figure 1) [34]. These properties can be estimated from the scientific literature, as well as through in situ and laboratory tests. On-site tests, such as the Thermal Response Test (TRT) [35], are a popular tool to measure the ground thermal conductivity in situ. The main drawback is that it is essential to ensure a minimal thermal interference between the surface and the GHE in order to obtain a correct interpretation of long-term results [10], which introduces further complexity to the test. Moreover, laboratory tests have been developed to determine the thermal properties of the soil under controlled scenarios. These include the guarded-hot-plate (GHP), the transient-hot-wire (THW) [36], the box probe, the dual-needle, and the single-needle methods [37]. These methods allow the direct measurement of the thermal properties of materials under both controlled temperature and humidity conditions. The difficulty in determining thermal properties within a SuDS lies in the fact that it is a porous medium, as well as a multilayer heterogeneous system made of varying materials, and therefore, governed by different and rather specific physical processes. As a consequence, determining the effective or equivalent thermal conductivity values of the SuDS technique should be one of the main objectives when working with such complexity in varying layers and physical processes [34].

In addition, previous research in the literature on the potential geothermal utilization of SuDS neither fully accounted for the physical thermal processes associated with the materials analyzed in the studied SuDS techniques, nor considered their energy-oriented design to include energetic parameters in the overall design exercise [14,34,35]. As a result, real-world field tests combining ground source heat pumps (GSHP) with PPSs have not performed as well as they should have as the hydrologic and water quality aspects ruled the design scheme and main targets. In this vein, the GHE was unduly influenced by

variations in ambient temperature, as this aspect had not been taken into consideration in the designs [38,39]. This research aims to address this gap in the existing literature by studying the thermal properties of a green swale, so that an energy-efficient design of combined SuDS–SGS systems can be achieved in the future for these "green" SuDS. With this aim, various materials with different configurations and operating conditions (dry and wet scenarios) were evaluated to propose a new methodology to achieve an optimal design of SuDS from an energy utilization perspective.

This study followed an experimental procedure used in previous research that examined the thermal properties of a blue roof to improve a building's thermal envelope [40]. Additionally, the thermal properties of materials comprising different types of green swale sections were determined. A non-destructive test was employed using the modified transient plane source (MTPS) method, also previously used by other researchers to study the thermal properties of materials used in geothermal systems [41,42].

Furthermore, numerical models of the studied green swales were created using a hybrid numerical–experimental methodology, as employed by other authors for studying the thermal behavior of construction systems [43]. These numerical models aim to further investigate the heat transmission mechanisms when combining an SGS with a dry swale. The specific objectives to achieve this goal are described below.

- Characterization of the thermal properties of the materials used in the green swale cross-sections.
- Identification and determination of the effect of the use of non-conventional materials such as expanded clay and construction and demolition waste (CDW) on the thermal behavior of a SuDS.
- Laboratory determination of the key thermal parameters of the different layers of the green swale sections by means of standardized tests, and analyzing their thermal behavior and their implications in a system combined with surface geothermal energy in dry and wet operating conditions.
- Validation of the results obtained in the laboratory tests by means of steady-state numerical simulations, Design of Experiments (DOE), and the use of Multi-Objective Genetic Algorithms (MOGAs).
- Simulation of the behavior of green swales in real operating conditions, using transient state numerical models.

2. Materials and Methods

2.1. Materials

Green swales, of the dry type, are essentially made of a series of layers: the surface layer, the filtering medium (usually made of engineered soil or aggregates), and the transition and draining layers placed at the bottom part of the cross-section [31,44]. The materials used in each one of these layers can vary depending on the main functionality targeted, the subsequent design, and the main hydrological and water treatment objectives set by the on-site requirements and constraints. In this research, three different cross-sections were studied using the following materials (the specific layers are shown in Table 1):

- **Material 1: Vegetable land (topsoil)** with an apparent density of 1400 kg/m^3. This material was used as the surface layer in all the studied models.
- **Material 2: Limestone aggregate** with a particle size of 0/32 mm, apparent density of 2690 kg/m^3, and porosity of 35%.
- **Material 3: Expanded clay** with a particle size of 10/20 mm, apparent density of 275 kg/m^3, and porosity of 34%. Expanded clay, due to its industrial manufacturing process, has a higher porosity, a lower density, and a vitrified surface [45].
- **Material 4: Mixed CDW** (combined recycled aggregate of mixed origin) 0/32, following the specifications the EN 13242:2Q02 + A1:2007 standard [46]. It has a particle density of 2.5 + 0.2 mg/m^3 and a water absorption rate of less than 7%.
- **Material 5: Infiltration cells**. A modular tank system that provides up to 90% void space and has a thickness of 52 mm was constructed through the use of the Atlantis

Flo-Cell® infiltration cell. The cells allowed efficient water drainage, while retaining an optimal moisture level for the overlying vegetative layers. This material was used as the drainage layer in all the models.

Table 1. Materials of the different green swales' sections.

Section	Thickness (mm)	Green Swale—Type 1	Green Swale—Type 2	Green Swale—Type 3
Top layer	100	Vegetable land	Vegetable land	Vegetable land
Intermediate layer	150	Limestone aggregates	Limestone aggregates	CDW
Sub-base	200	Limestone aggregates	Expanded clay	Expanded clay
Lower layer	52	Infiltration Cells	Infiltration Cells	Infiltration Cells

Three different sections of dry swales were constructed by combining the aforementioned materials as can be seen in Table 1.

A geotextile was placed between all the interfaces of the different layers, with the aim of serving as a transition layer between them. The geotextile used is made of 150 g/m^2 short polyester fibers, which are not inter-woven. It has a thickness of 1.0 ± 0.2 mm.

2.2. Materials Characterization

In addition to the properties of the materials provided by the suppliers, a series of laboratory tests were conducted for a more extensive and detailed characterization for the purposes of this experiment. These tests involved performing a particle size analysis according to the UNE-EN 933-1:2012 standard [47]. Thus, the particle size distribution curves of the different materials were obtained (see Table 2).

Table 2. Particle size distribution of the materials.

	Sieve	40	31.5	22.4	16	11.2	8	5.6	4	2	1	0.5	0.25	0.063
CDW	% pass	100.0	95.0	62.0	60.0	50.0	40.0	36.0	30.0	20.0	16.0	15.0	10.0	5.0
Vegetable land	%pass	100.0	100.0	100.0	100.0	100.0	89.0	78.0	71.0	56.0	44.0	35.0	21.0	3.0
Expanded clay	%pass	100.0	100.0	100.0	100.0	95.0	59.0	25.0	1.9	1.0	0.0	0.0	0.0	0.0
Limestone aggregates	%pass	100.0	94.0	77.5	69.8	64.0	51.5	41.9	35.5	23.5	17.2	14.0	10.0	4.5

The values of the thermal conductivity of the materials were determined by means of a TCI analyzer from C-Therm®, which is a non-destructive test based on the MTPS technique as specified in the UNE-EN ISO 22007-2:2023 [48] and ASTM D7984:21 standards [49]. This technique employs a reflective sensor that applies a constant and instantaneous heat source on the test specimen. The equipment allows for direct measurements of thermal conductivity and thermal effusivity of powders, liquids, gels, and solid materials, the latter ones being the targeted material for this research. To perform the tests, a standard weight is placed on the samples to ensure contact with the sensor. Furthermore, in the tests with solids (such as the limestone aggregate in this study), a contact paste (Wakefield thermal

joint compound type 120 silicone) was used to eliminate gaps between the sensor and the sample.

Three samples of each material (limestone aggregate, topsoil, recycled aggregates, and expanded clay) were taken in order to perform the tests. The expanded clay was crushed to form a homogeneous powder, as was the topsoil. In the case of the limestone and recycled aggregates, three samples were taken and used to create three stone slabs with two flat sides (see Figure 2).

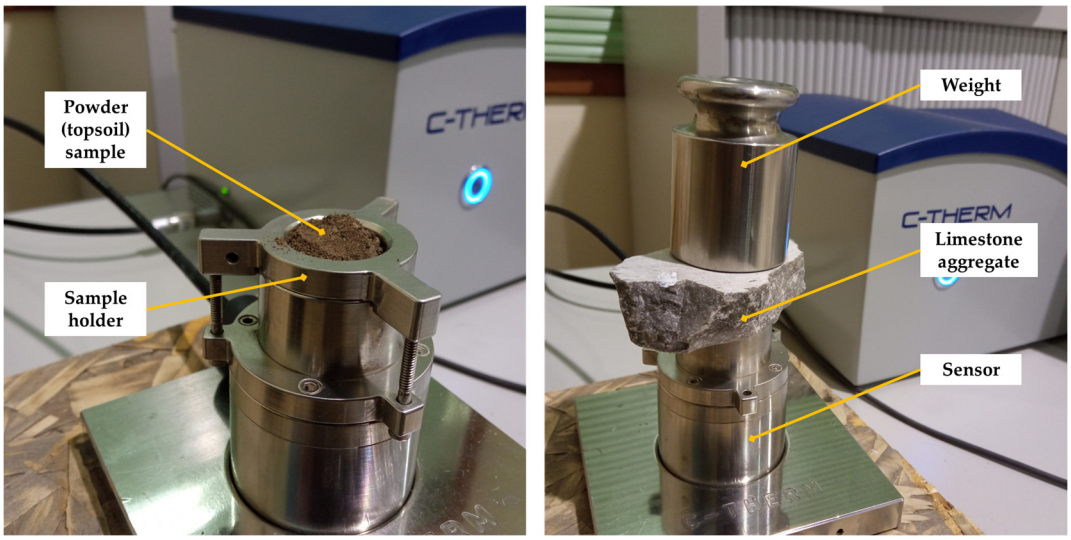

Figure 2. Measurement of thermal conductivity with C-Therm® TCI analyzer: powder test (**left**) and solid test (**right**).

The tests were performed under two different scenarios:

- Ambient conditions, with the materials tested under laboratory-controlled temperature and relative humidity (RH): T = 18.5 ± 0.5 °C and RH = 80%.
- Wet conditions, where the materials were tested under saturated conditions. In the case of the expanded clay and topsoil layers, water was added gradually until a soft consistent paste was formed. For the limestone aggregate specimens, they were immersed in a container with water at a constant temperature of 22.4 ± 0.5 °C for 168.0 ± 0.5 h until they reached full saturation.

The tests were carried out with constant mass specimens, following the standard procedure depicted in UNE-EN 1097-6: 2014 [50] in all scenarios. A constant mass was achieved after successive weightings at least 1 h apart until the mass did not differ by more than 0.1%.

Six tests were developed for each material under each condition (two tests for each sample of material), resulting in a total of 16 tests per material (8 under ambient conditions and 8 under wet conditions). In addition, 10 measurements were taken in each test, resulting in a total of 80 measurements for each condition. The directly measured values of thermal effusivity (Ef) and thermal conductivity (λ) have a precision greater than 1% and an accuracy greater than 5%, according to the equipment specifications. For data processing, the values of the two extreme tests out of the tests conducted for each condition were not considered. Specific heat was calculated using the thermal effusivity, the thermal conductivity, and the density of the material (ρ) by means of Equation (1):

$$C_p = {Ef^2} \Big/ {\rho \cdot \lambda} \quad (1)$$

The average value of the readings from the remaining tests with intermediate values was taken to obtain the values shown in Table 3.

Table 3. Thermal properties of the measured materials.

Material	Ambient Conditions				Wet Conditions		
	ρ (kg/m^3)	λ (W/mK)	Ef (Ws$^{1/2}$/m^{2}K)	C_p (J/kgK)	λ (W/mK)	Ef (Ws$^{1/2}$/m^{2}K)	C_p (J/kgK)
Vegetable land	1370	0.1422	449.89	1039	1.4121	1646.58	1280
Limestone aggregate	2400	1.8983	1721.66	651	2.3253	2081.07	745
Recycled aggregate	2100	1.4876	1473.48	695	2.0827	1901.03	723
Expanded clay	500	0.0982	309.58	1952	0.7101	921.95	1995

2.3. Experimental Set-Up

The equipment used to conduct the thermal characterization tests in the laboratory under steady-state conditions consists of the following elements (see Figure 3):

- Climatic generator: This equipment allows for precise control of relative humidity and temperature values in an enclosed environment, ensuing constant cold, heat, and humidity.
- Calibrated hot-box: A fully insulated 1 m^3 capacity hot-box is connected to the climatic generator equipment (see Figure 3). The calibrated hot-box is used to create an environment under controlled temperature and humidity conditions for each test. The above-mentioned equipment operates as indicated in the UNE-EN ISO 8990:1997 [51] and ASTM C1363:19 standards [52].
- Test-box: This is the container in which the tested green swale cross-sections were introduced and set up according to the experimental procedure. It has interior dimensions of 608 $\times$ 408 mm^2 at the bottom. The test-box is installed over the hot-box (see Figure 3) so that the heat flux passes perpendicularly through the surface of the studied green swale cross-section from its bottom layer. The test-box is thermally insulated from the outside with 20 cm of extruded polystyrene (0.033 $\pm$ 0.003 W/mK) in order to minimize lateral heat losses.

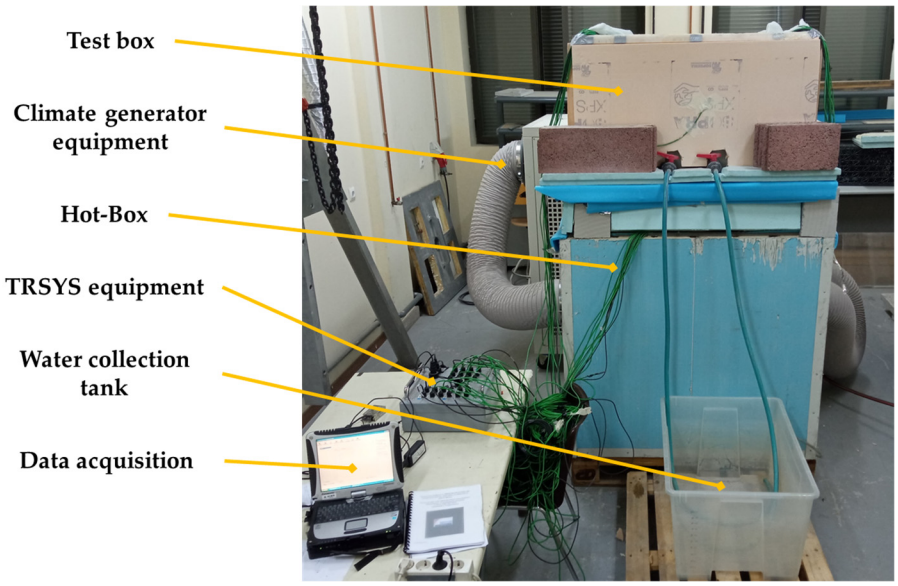

Figure 3. Experimental set-up depicting the climatic generator equipment, the calibrated hot-box, and the test box.

For measuring the parameters and collecting and storing the data, the following equipment and sensors were used:

- Temperature and heat flux sensors: Fourteen type K thermocouples (TCxy) were installed according to the distribution shown in Figure 4. Additionally, two extra thermocouples were used to determine the heat loss through the walls of the Test-box. Eight thermal flux sensors (HFx) Hukseflux HFP01 were employed, and they were installed at the interfaces of all the layers (see Figure 4). The technical specifications of the thermal flux sensors are as follows: sensitivity, 60×10^{-6} V/(W/m^2); thermal resistance of the sensor, 71×10^{-4} K/(W/m^2); nominal operating temperature range, -30 to +70 °C; and measurement range, -2000 to +2000 W/m^2.
- TRSYS equipment: This system was used to acquire data from the aforementioned sensors, and it was programmed to collect information in 10 min interval. It also allows for data storage and transmission for further analyses.

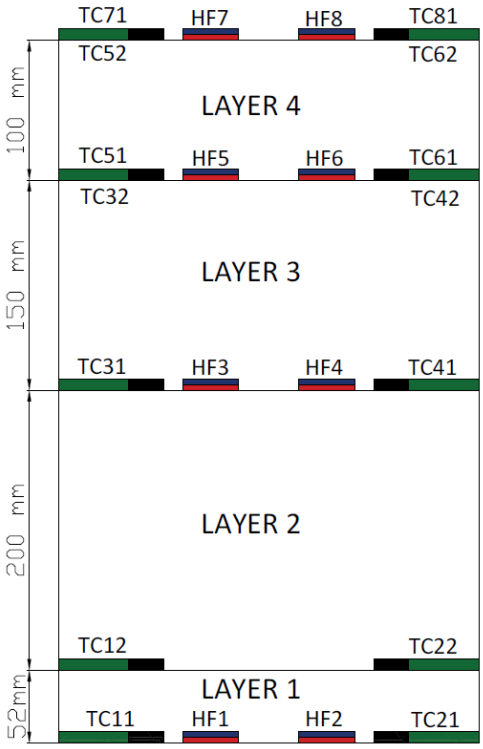

Figure 4. Distribution of the temperature and heat flux sensors within the green swale cross-section.

2.4. Calculation of the Thermal Conductivity: Physical Principles

Heat is transmitted mainly by three widely studied thermal mechanisms: conduction, convection, and radiation. In the subsurface, the main heat transfer mechanism is conduction [53]. Heat transfer by conduction, in an isotropic medium and under stationary conditions, is described by Fourier's Law. Applying Fourier's Law for one dimension, we obtain Equation (2).

$$q_x = \lambda_x \times \nabla T \tag{2}$$

where

q_x [W $*$ m^{-2}] represents the heat flux.

λ_x [W $*$ k^{-1} $*$ m^{-1}] stands for the thermal conductivity in the x direction.

∇T[K $*$ m^{-1}] indicates the thermal gradient between the heat source and the heat sink.

It also can be expressed as follows (Equation (3)):

$$\nabla T = \frac{dT}{dx} \cong \frac{\Delta T}{x} \tag{3}$$

where

ΔT [K] is the temperature differential.

x [m] represents the total thickness of the green swale model.

Since the values of heat flux and temperature gradient have been registered in the laboratory, the equivalent thermal conductivity was directly computed as it is the constant ratio between the two of them. In addition, the thermal transmittance (U) can be obtained by applying Equation (4):

$$U[\mathrm{W} * \mathrm{k}^{-1} * \mathrm{m}^{-2}] = q_x / \Delta T \quad (4)$$

Convective heat transfer, on the other hand, occurs across the boundaries between the different layers. If radiative heat transfer is not taken into account, the heat transfer by conduction between two surfaces can be defined as follows (Equation (5)) [54]:

$$q_{TCC} = k_{TCC} * (T_{c,T} - T_{c,C}) \quad (5)$$

where

q_{TCC} $[\mathrm{W} * \mathrm{m}^{-2}]$ represents the heat flux in the interface.

$k_{TCC}[\mathrm{W} * \mathrm{m}^{-2} * {}^{\circ}\mathrm{C}]$ stands for the thermal conductivity coefficient at the contact interface. Previous research suggests a value of 2 $\mathrm{kW/m^2\ ^{\circ}C}$ [54].

$T_{c,T}$, $T_{c,C}$ [°C] are the contact point temperatures registered in the target and the contact surfaces, respectively.

2.5. Experimental Methodology

The three sections of the dry swale were tested under two operating scenarios: dry and wet, which are extremes in their standard hydrological performance. In the dry condition test, the materials forming the cross-sections (see Figure 4) were placed within the test-box and tested without the presence of water. Once the dry test was finalized, the dry swale section was fully saturated by pouring water into the test-box until a constant layer of water was reached over the top surface of the swale model. Thereupon, the swale laboratory model was kept under saturated conditions for 36.0 ± 0.5 h to ensure no variation in the layer of water on the surface. After this saturation period, all the water was removed from the test-box, and the thermal characterization test was conducted under wet conditions. Table 4 shows the values of the volumes of water added to each dry swale cross-section, as well as the volume of water extracted and absorbed by each section.

Table 4. Hydraulic capacity for each green swale model registered with an error of ± 0.5 L.

Green Swale	Volume of Water Discharged (L)	Volume of Water Extracted (L)	Volume of Water Absorbed (L)
Type 1	122.7	99.3	23.4
Type 2	152.6	113.6	39.0
Type 3	146.1	108.5	37.6

In addition, the climatic generator equipment was programmed to gradually increase the temperature from the initial baseline at 20 °C, which corresponds to the laboratory's ambient temperature, to a final stabilization temperature of 55 °C. This heating process was carried out by using a series of thermal ramps to ensure a stable thermal flow during the process. The initial temperature increase stage took approximately 24 ± 0.5 h.

The temperature gradient between the top and the bottom layers of the dry swale models should be greater than 15 °C, so that the values obtained for transmittance and equivalent thermal conductivity could be considered reliable as indicated in the UNE-EN ISO 8990:1997 [51] and ASTM C1363:19 [52] standards, which serve as the methodological framework to this type of test. Therefore, a temperature of 55 °C was selected for the tests in order to ensure that this temperature difference was achieved in all the studied models.

The total duration of each test was 144.0 ± 0.5 h. The values of the thermal performance of the cross-sections were recorded during the last 24 ± 0.5 h of the test, as it was considered the time when the system had stabilized.

2.6. Numerical Models

The Finite Element Analysis (FEM) with two-dimensional (2D) models of the examined cross-sectional areas were applied using the ANSYS Workbench 2023 R2 software. A 10 mm mesh size was computed using hexahedral plane elements (PLANE293) with 8 nodes and one degree of freedom for the temperature parameter. This element is considered appropriate for this type of analysis as suggested by previous research [55]. The inflation tool was utilized to minimize the mesh size in the layers' contact areas with a maximum thickness of 5 mm, obtaining 10 layers and a growth rate of 1.2. A sensitivity analysis of the mesh was carried out to study whether the element size influenced the results achieved from the models.

2.6.1. Steady-State Thermal Model

Firstly, an analysis of the steady-state behavior of the green swale sections, both under dry and wet conditions, was conducted. This modeling sought to replicate the laboratory conditions to obtain the optimized thermal conductivity values in all materials utilized in the laboratory models. This stationary model simulates the concept used in previous investigations for this sort of analysis [40].

This procedure was carried out using a semi-adiabatic approach for the side walls of the cross-sections, assuming lateral heat losses of 6W in the test-box. A convection model was implemented over the top surface of the model, assuming an ambient temperature of 20 °C and a convective surface coefficient of 5.0 W/K m^2, following the guidelines established in Annex C of the UNE-EN ISO 6946:2021 [56] standard. The experimental temperature measurements registered at the top and bottom points of the swale laboratory models were used as input data for the previously validated FEM model [57], which yielded errors below 2%.

The equivalent thermal conductivities of each layer of the laboratory models were optimized using a multi-criteria method based upon the DOE [58] after the experimental results of the thermal behavior of the cross-sections were analyzed. Objectives and constraints were established in the MOGA [59]. The design variables, such as the input and output parameters for conducting the DOE, were defined considering the temperature conditions and the heat flux transfer registered in the experimental tests. Constructing a response surface allowed for accurate predictions. Finally, using the MOGA, the optimal equivalent thermal conductivity values of the dry swale materials were determined using the defined search ranges on the response surface. The thermal transmittance results obtained experimentally were used as objectives in the optimization process. In this vein, the MOGA achieved optimal solutions that appropriately fit the experimental data.

2.6.2. Transient Thermal Model

Subsequently, a transient analysis of the model was performed to reproduce the thermal behavior of the dry swales in real operating conditions. There were slight differences from the boundary conditions used in the stationary analysis. The transient temperature curve (10 days) shown in Figure 5 was introduced at the top of the model, simulating the standard ambient temperature for a typical summer in northern Spain [60]. In addition, a symmetry function was added to the side walls of the model (x-direction), so that they are continuous. The heat dissipation that would occur in real operating conditions was simulated at the bottom of the model. The thermal conductivity values of the materials used were those obtained with the MOGA analysis in the previous steady-state model. The values of the materials' specific heats used in the numerical models are those obtained by the MTPS technique and shown in Table 3.

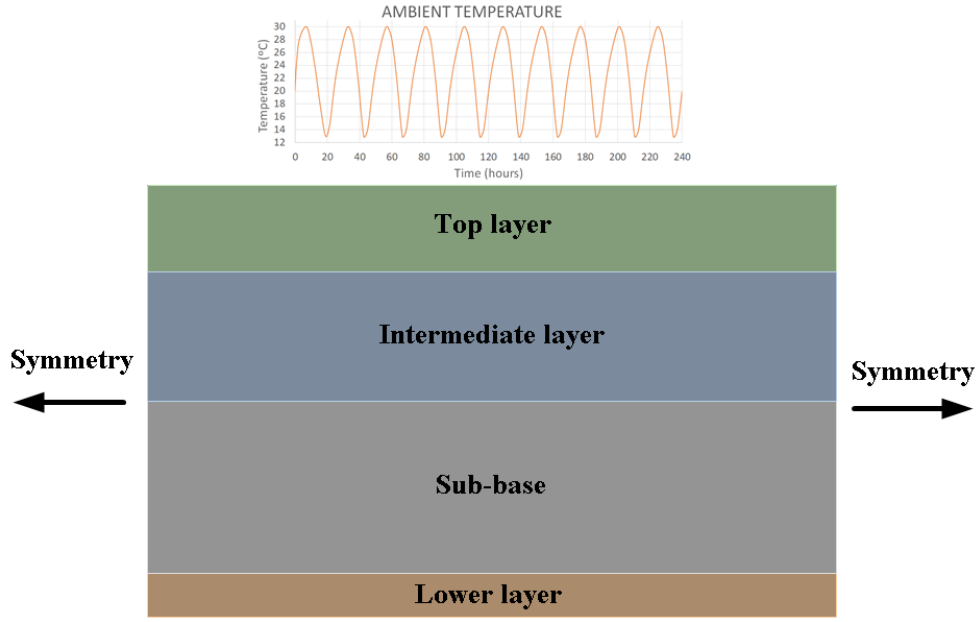

Figure 5. Boundary conditions for the transient model.

3. Results and Discussion

3.1. Experimental Results

The difference in temperatures between the top and the bottom layers of the green swale sections is presented in Figure 6. The differences are rather similar in all tests except for the type 1 cross-section under wet conditions, which may be indicative of its lower thermal insulation capacity compared to the sections incorporating lightweight aggregates. Moreover, this fact meets the requirement set by the standards [51,52] regarding keeping a difference in temperature of at least 15 °C in order to obtain reliable data from the tests.

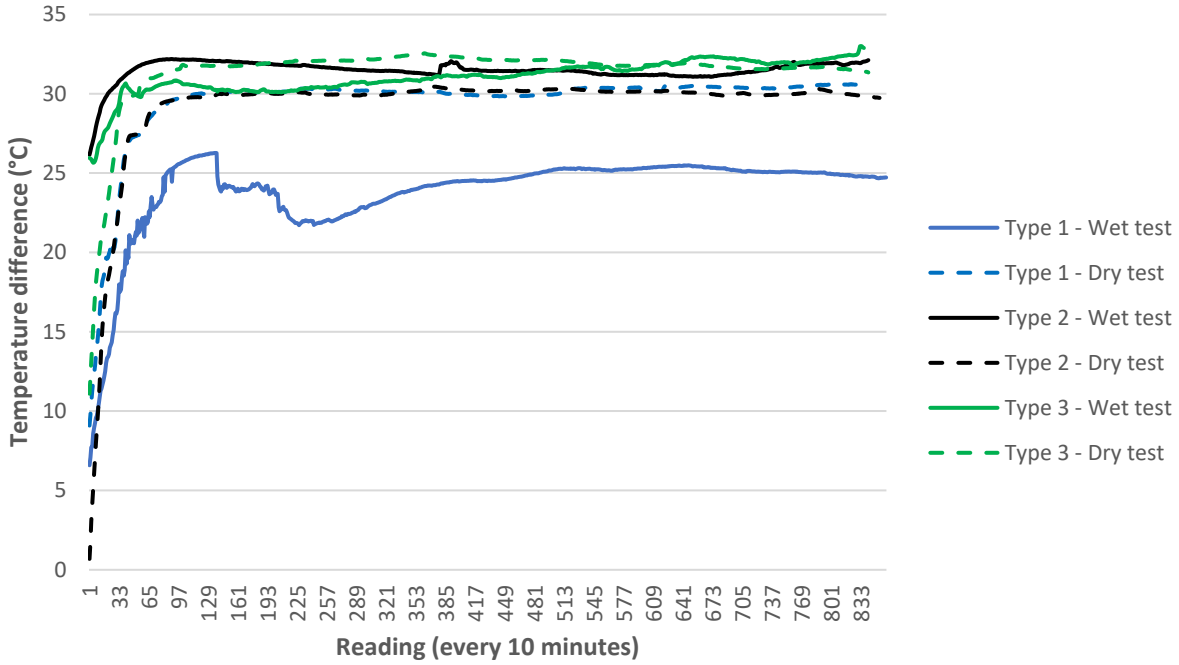

Figure 6. Difference in temperature during the whole test between the bottom and the top part of the green swales under dry and wet conditions.

The thermal transmittance values were recorded during the last 24 h of the test once the system had stabilized (see Table 5). Model type 1, consisting of limestone aggregate, exhibited the worst thermal performance; while model type 2, using expanded clay, and model type 3, incorporating both expanded clay and CDW, demonstrated a better thermal insulation capacity. Thus, these two models provided the most favorable thermal properties for the potential water–energy integration through the incorporation of GSHP elements housed by this SuDS and working under the aforementioned hydrologic scenarios.

Table 5. Average values, absolute error, relative error, and sample standard deviation (S) of the thermal transmittance of the green swale sections.

Green Swale	Dry Conditions				Wet Conditions			
	U (W/m^2K)	Absolute Error (W/m^2K)	Relative Error (%)	S (W/m^2K)	U (W/m^2K)	Absolute Error (W/m^2K)	Relative Error (%)	S (W/m^2K)
Type 1	0.631	0.018	3.36	0.021	0.911	0.046	5.16	0.050
Type 2	0.347	0.020	6.20	0.025	0.558	0.006	1.29	0.007
Type 3	0.338	0.014	4.86	0.016	0.602	0.014	3.69	0.016

Furthermore, the presence of water in the system, replicating the functioning of a green swale during intense storm events, negatively affected its thermal performance. Figure 7 shows the values of the green swale equivalent thermal conductivity recorded during the last 24 h of the test. It can be observed that the test carried out under the wet conditions in model type 1 exhibited more variability in the values and also resulted in the lowest temperature difference compared to the other tests.

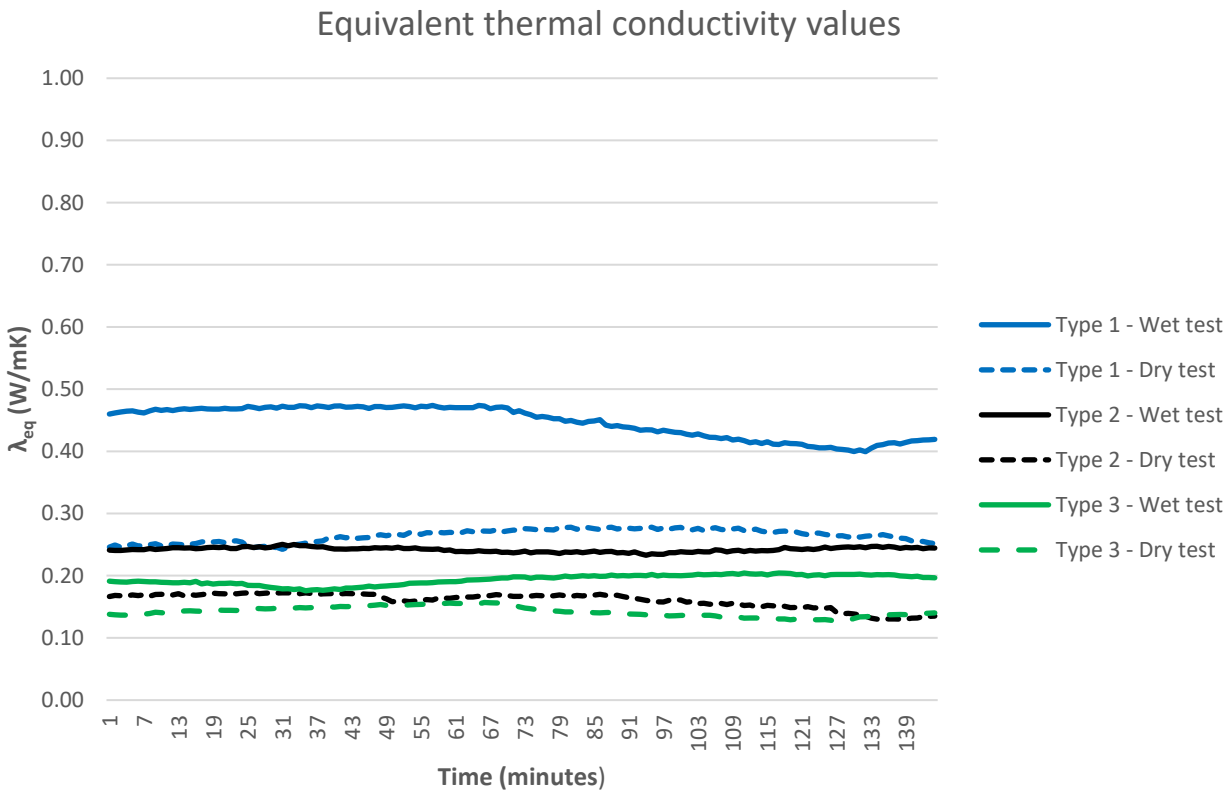

Figure 7. Equivalent thermal conductivity values of the green swale sections during the last 24 h of the experiments under dry and wet conditions.

Table 6 presents the values of the averaged equivalent thermal conductivities for each of the analyzed dry swale types under both wet and dry conditions. All the values showed

low relative errors, with 6.20% as the highest value computed. The type 1 section (representing the conventional design) showed poorer thermal insulation capacity compared to type 2 and type 3 cross-sections. It is also noticeable that the thermal performance of all dry swale models was worse under wet conditions in comparison to dry conditions (see Table 6).

Table 6. Average values, absolute error, relative error, and sample standard deviation (S) of the equivalent thermal conductivity of the green swale sections.

Green Swale	Dry Conditions				Wet Conditions			
	λ_{eq} (W/mK)	Absolute Error (W/mK)	Relative Error (%)	S (W/mK)	λ_{eq} (W/mK)	Absolute Error (W/mK)	Relative Error (%)	S (W/mK)
Type 1	0.284	0.009	3.36	0.010	0.410	0.023	5.16	0.025
Type 2	0.156	0.010	6.20	0.012	0.251	0.003	1.29	0.004
Type 3	0.152	0.007	4.86	0.008	0.271	0.007	3.69	0.008

It is important to mention that other authors such as Sivaprasad and Basu [61] calculated the thermal properties of various types of soil, and their values were less favorable than those obtained in the type 2 and 3 green swale models. This suggests that the thermal insulation capacity provided by these materials and particular sections was higher than that of conventional soils. Therefore, the greater thermal insulation provided by designed green swales will positively affect the performance of GHEs, potentially leading to an improvement in their efficiency. Designing SuDS techniques incorporating an energy perspective to the four pillars of SuDS design has proven to provide an enhancement of the geothermal system compared to a conventional installation.

Further to this, Table 7 shows the averaged values obtained for each material. In most cases, a difference of 15 °C between the top and bottom parts on each layer was not achieved, so these values are not supported by the recommendations provided in the standards for these tests. Moreover, differences between these values and those obtained using the MTPS technique (see Table 3) were observed. The reason for this was that the materials placed inside the green swales have a heterogeneous arrangement with the presence of air and water (the latter occurring in the wet tests).

Table 7. Values of the averaged equivalent thermal conductivity of the material layers under dry and wet conditions.

Thermal Conductivity (W/mK)	Dry Conditions	Wet Conditions
Vegetable land	0.396	1.386
Limestone aggregates	0.268	0.816
Expanded clay	0.147	0.359
CDW	0.291	1.416

It was not possible to evaluate the effect of the surface vegetation and the evapotranspiration on the thermal performance of the green swale due to the operational constraints of the testing procedure. Also, this vegetation is believed to contribute to the improvement of the thermal properties of the green swales according to previous research [13].

3.2. Numerical Results

3.2.1. Mesh Sensitivity Analysis

A sensitivity analysis of the mesh was carried out by applying DOE techniques. The objective was to evaluate the parameters with the greatest influence on the model to obtain a better correlation between the experimental values and those computed numerically. The face sizing element size, inflation number of layers, inflation growth rate and inflation

maximum thickness, were evaluated. It was noted that the face sizing element size, with a local sensitivity of 50%, was the most influential parameter. The influences of the other parameters were lower, all of them showing local sensitivity values below 5%.

As shown in Figure 8, the result of the mesh sensitivity analysis indicates that the maximum difference in thermal transmittance values for different mesh sizes was less than 0.02%. Therefore, the value of 10 mm was applied, since previous work has also recommended this mesh size for this type of study [40].

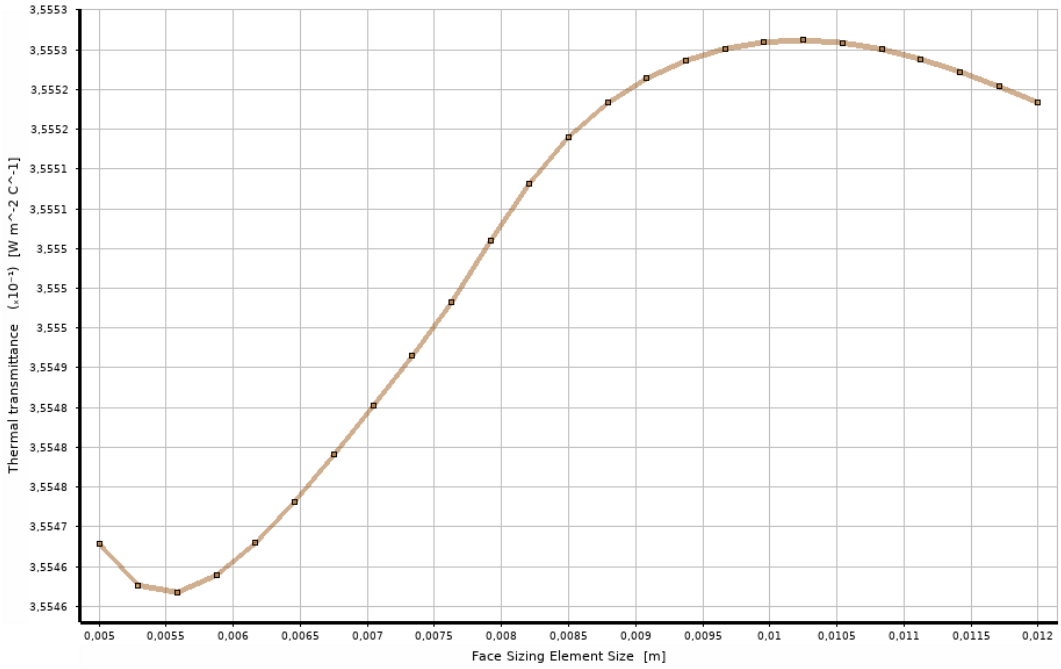

Figure 8. Mesh sensitivity analysis: effect of face sizing element size.

3.2.2. Steady-State Thermal Model Results

The steady-state analysis was performed by means of the DOE analysis, where a series of search ranges were established (see Table 8). These ranges correspond to a deviation of ±50% of the values measured in the laboratory (see Table 7).

Table 8. Search ranges for the equivalent thermal conductivities of the materials of the green swale layers.

Thermal Conductivity (W/mK)	Dry Conditions		Wet Conditions	
	Lower Bound	Upper Bound	Lower Bound	Upper Bound
Vegetable land	0.20	0.59	0.69	2.08
Limestone aggregates	0.13	0.40	0.41	1.22
Expanded clay	0.07	0.22	0.18	0.54
CDW	0.15	0.44	0.71	2.12

Once the search ranges for each of the materials had been configured, the objective function of the MOGA was set to obtain the empirical thermal conductivity values (see Table 5). In this vein, the optimized values of the equivalent thermal conductivity of the materials were obtained (see Table 9). As it can be seen, there were variations between the optimized values and the values measured in the laboratory, since some of the values of the materials measured in the laboratory were not endorsed by the standards.

Table 9. Optimized equivalent thermal conductivity values of the materials of green swale layers.

Thermal Conductivity (W/mK)	Dry Conditions	Wet Conditions
Vegetable land	0.373	0.963
Limestone aggregates	0.348	0.795
Expanded clay	0.105	0.298
CDW	0.315	0.711

3.2.3. Transient Thermal Model Results

The first finding that has been observed in the transient thermal models was the importance of positioning the expanded clay layer appropriately within the green swale cross-section. As it can be seen in Figure 9, the thermal insulation reached at the lower part of the type 2 model under dry conditions was greater than the one registered when introducing the expanded clay in the intermediate layer instead of in the sub-base layer. This change in the cross-section arrangements of the dry swale layers would reduce the temperature in the area where the shallow geothermal conduits should be placed; after 10 days, it was as much as 0.535 °C below the value of the cross-section with the expanded clay placed in the sub-base.

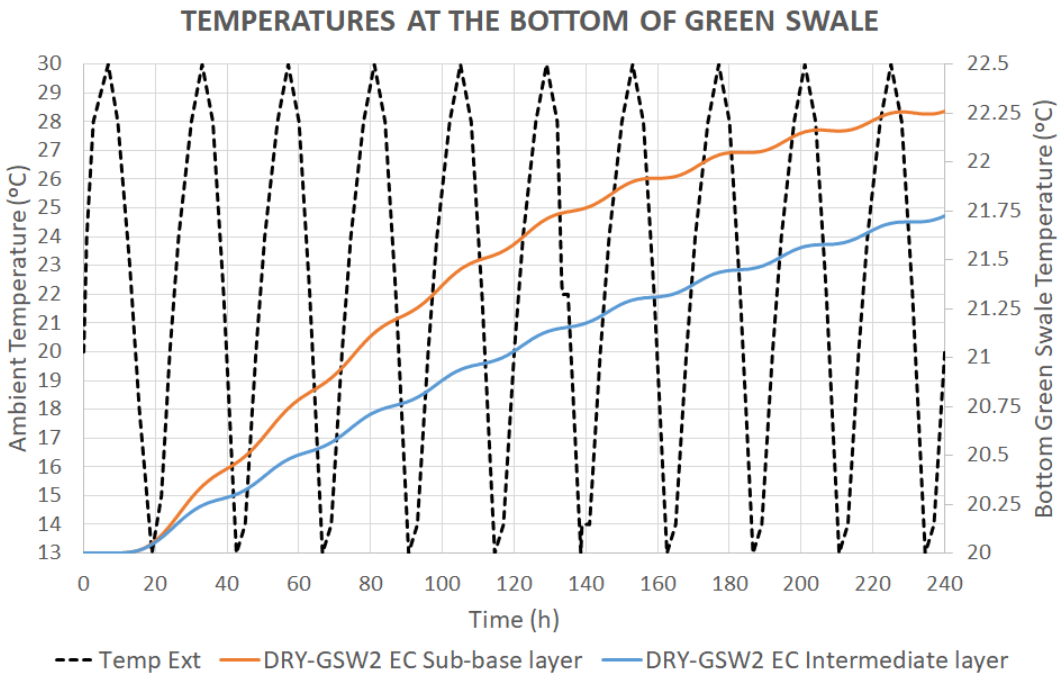

Figure 9. Temperatures at the bottom layer in type 2 green swale models under dry conditions based on the final location of the expanded clay within the cross-section.

Therefore, the expanded clay in types 2 and 3 should be placed in the intermediate layer and the limestone aggregate and CDW is recommended to be placed in the sub-base layer.

Figures 10 and 11 show the evolution of the temperature values at the bottom of green swales under dry and wet conditions, respectively. In both cases, it is possible to observe the improvement in the insulation capacity of the ground regarding with the outside ambient temperature in the dry swales in which expanded clay is used. On the one hand, the performance of type 2 and 3 green swales under dry conditions is reported to be rather similar, presenting final temperatures of 21.72 °C and 21.77 °C, respectively, which are lower than those registered in type 1 (22.27 °C). On the other hand, the drop in thermal insulation performance of the ground can be particularly noticed for the models performing under

wet conditions. Likewise, it should also be highlighted that there were greater temperature variations at the bottom of the swales functioning under wet operating conditions, which will be more influenced by the ambient conditions outside. Temperatures of 22.78 °C, 22.52 °C, and 22.54 °C were reached for types 1, 2, and 3 model swales, respectively, under wet conditions.

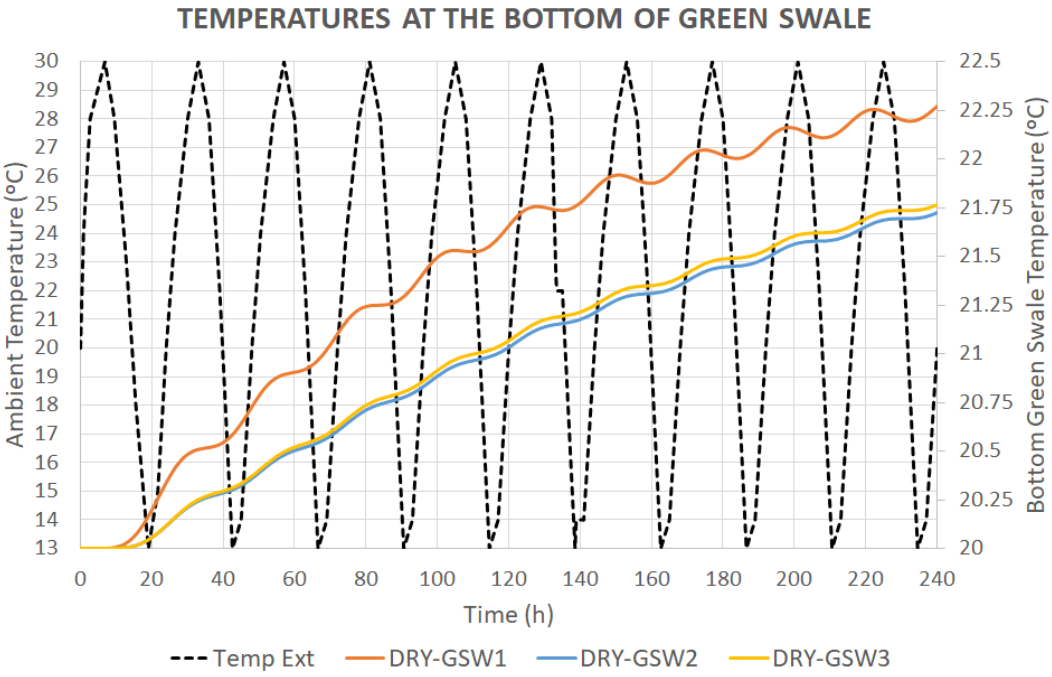

Figure 10. Comparison of the temperatures registered at the bottom of the dry swale with the ambient temperatures under dry conditions.

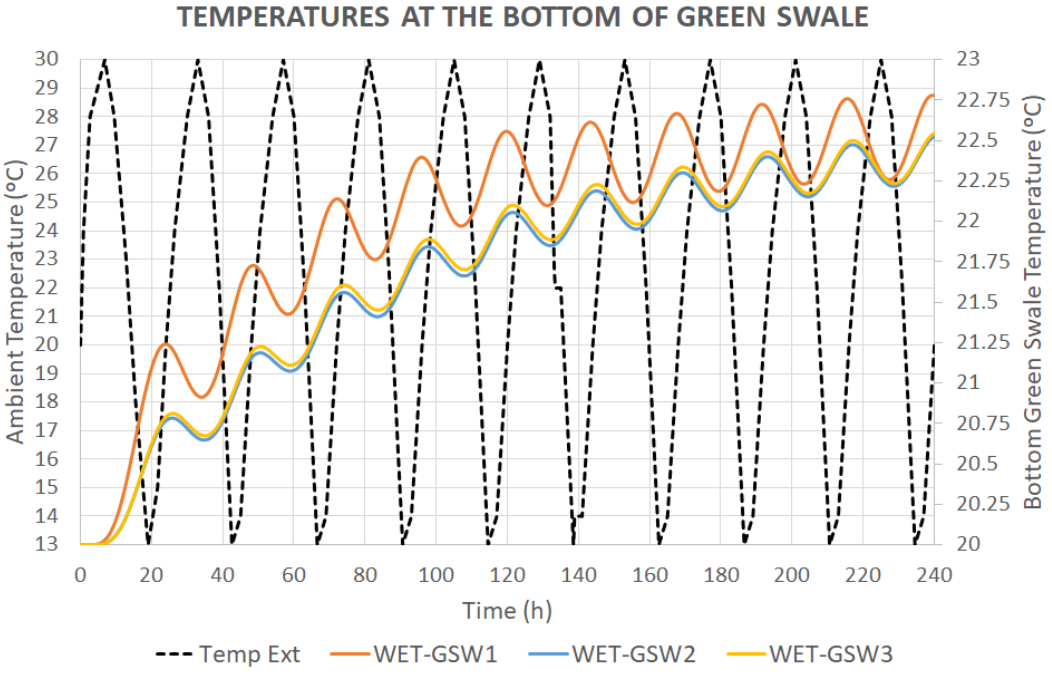

Figure 11. Comparison of the temperatures registered at the bottom of the green swale with the ambient temperatures under wet conditions.

The temperature in the lower part of the swales (where the GHE would be placed) increases during a 10-day period. The main reason is the accumulation of heat in the lower area close to the heat exchanger. In order to study this phenomenon correctly, it will be necessary to carry out field tests to help determine the dissipative effect of the soil under the dry swale and thus allowing for the calibration of the developed models.

Even so, the temperature difference between the bottom of the swale and the ambient temperature was significant. In the worst scenario reported in this study, an increase of 2.77 °C in comparison with the initial temperature of 20 °C was registered at the bottom of the dry swale (see Table 10). A higher temperature difference between the ambient temperature and the GHE temperature would result in better performance of the GSHP [34].

Table 10. Temperature increases (°C) registered at the bottom of green swale models.

Green Swale	Dry Conditions	Wet Conditions
Type 1	2.270	2.776
Type 2	1.772	2.522
Type 3	1.765	2.544

4. Conclusions and Future Research Directions

The present research adds knowledge to the existing gap regarding the energy utilization of SuDS. Therefore, a novel hybrid experimental-numerical methodology has been proposed to determine the thermal properties of entire cross-sections of SuDS, using a dry swale as the first SuDS technique to validate the methodology. This will enable a holistic design of swales in combination with shallow geothermal systems, incorporating the energy viewpoint and paving the way in the field for further experimentation in other SuDS.

The study also evaluated the inclusion of new materials in the cross-section of a green dry swale (expanded clay and CDW). It was observed that the implementation of these materials improved the swale's thermal properties. The equivalent thermal conductivity of the most favorable swale cross-section (model type 3) for implementing an SGS was found to be 0.152 W/mK under dry conditions and 0.271 W/mK under wet conditions. These values represent an 87% improvement under dry conditions and a 51% improvement under wet conditions compared to the equivalent thermal conductivity of the conventional green swale cross-section. In addition, the type 2 and 3 sections, formed by expanded clay, had a greater hydraulic storage capacity than the conventional section. This again highlights the importance of the energy–water nexus.

It has been observed that the thermal properties of the thermally designed SuDS has the potential to improve the performance of the GSHP compared to a conventional SGS installation in conventional soils.

Complementary tests were carried out to thermally characterize the materials used in the green swale; these were based on a non-destructive test using the MTPS method. The results obtained confirm that the actual thermal conductivity values of the materials, measured with traditional techniques, do not reproduce the real thermal behavior of swales. This is due to the fact that the materials and their arrangement are heterogeneous and other heat transfer phenomena occur between the green swale layers and their environment.

Transient numerical models have been shown to be a useful tool to simulate the thermal insulation capacity of SuDS under real climatic conditions to improve green swale designs. This will allow us to determine their impact on the performance of geothermal heat pumps when combined with SGS, since one of the fundamental design parameters is the temperature at which the GHE is located in the ground [34]. This will help to avoid design errors identified in field tests carried out by other authors, thus improving the performance of GSHP [18,24,39]. Future developments of simplified tools will allow engineers and specialists to determine the best possible design for these systems for the geothermal utilization of SuDS infrastructures.

As future research steps, field tests should be conducted to evaluate the thermal performance of the combined system of a green swale and a GHE in real conditions. With these field tests, it will be possible to validate the transient models. Additionally, the energy-driven SuDS design performance improvement should be assessed in the field. Hydraulic performance tests and water quality testing for the proposed SuDS designs should also be carried out to strengthen the water–energy nexus. Evaluating other SuDS typologies, as well as the use of different materials and cross-section types, would be enlightening. Lastly, the proper performance of the heat pump under this operating scenario should be tested in a real installation.

Author Contributions: Conceptualization, F.P.Á.-R., C.R.-M. and L.Á.S.-F.; methodology, C.R.-M. and F.P.Á.-R.; software, F.P.Á.-R. and C.R.-M.; validation, F.P.Á.-R. and C.R.-M.; formal analysis, C.R.-M. and F.P.Á.-R.; investigation, C.R.-M., F.P.Á.-R. and L.Á.S.-F.; resources, C.R.-M., F.P.Á.-R. and L.Á.S.-F.; writing original draft preparation, C.R.-M., F.P.Á.-R. and L.Á.S.-F.; writing—review and editing, F.P.Á.-R., C.R.-M. and L.Á.S.-F.; supervision, F.P.Á.-R. and L.Á.S.-F.; project administration, F.P.Á.-R., L.Á.S.-F. and C.R.-M.; funding acquisition, F.P.Á.-R., L.Á.S.-F. and C.R.-M. All authors have read and agreed to the published version of the manuscript.

Funding: This investigation was supported by the FICYT under the GRUPIN project, with the grant number SV-PA-21-AYUD/2021/51328, which was co-financed with EU FEDER funds. Carlos Rey-Mahía acknowledges the University of Oviedo for a Predoctoral Grant, reference PAPI-22-PF-8.

Institutional Review Board Statement: Not applicable.

Informed Consent Statement: Not applicable.

Data Availability Statement: The data presented in this study are available on request from the corresponding author. The data are not publicly available due to an ongoing research project, which provided part of the funding of this study.

Acknowledgments: The authors express gratitude to SUDS S.L. and Atlantis Corp for the provision of the lightweight modular tank structural systems used to test the cross-sections models in the laboratory. They extend their appreciation to Weber Saint-Gobain for the technical assistance and materials used in the realization of the models. Lastly, they thank Swanson Analysis Inc. for allowing the use of the university research version of the ANSYS 2023 R2 program in this paper.

Conflicts of Interest: The authors declare no conflict of interest. The funders had no role in the design of the study; in the collection, analyses, or interpretation of data; in the writing of the manuscript; or in the decision to publish the results.

Nomenclature

Acronyms

CDW	Construction and demolition waste
DOE	Design of Experiments
EU	European Union
FEM	Finite Element Analysis
GHE	Geothermal Heat Exchanger
GI	Green infrastructure
GSHP	Ground-source heat pump
GHP	Guarded-hot-plate
LID	Low impact development
MIT	Massachusetts Institute of Technology
MTPS	Modified transient plane source
MOGA	Multi-Objective Genetic Algorithm
NBS	Nature-based solutions
PPS	Permeable Pavement Systems
SCM	Stormwater constructed measures
SDGs	Sustainable Development Goals
SGS	Shallow geothermal system
SuDS	Sustainable Drainage System

TRT	Thermal Response Test
THW	Transient-hot-wire
UN	United Nations

Symbols

U	Thermal transmittance (W/m^2K)
ΔT	Temperature differential (K)
∇T	Thermal gradient between the heat source and the heat sink (K/m)
q_x	Average heat flux (W/m^2)
RH	Relative humidity (%)
S	Sample standard deviation
x	Total thickness of the green swale model (m)
λ_x	Thermal conductivity in the x direction (W/mK)
λ_{eq}	Equivalent thermal conductivity (W/mK)
q_{TCC}	Heat flux per unit area in the interlayer (W/m^2)
k_{TCC}	Thermal contact conductance coefficient ($W/m^2{}^\circ C$)
$T_{c,T}$; $T_{c,C}$	Temperatures of the contacts points (°C)
ρ	Density of the material (kg/m^3)
Ef	Thermal effusivity ($Ws^{1/2}/m^2K$)
Cp	Specific heat (J/kgK)

References

1. International Energy Agency (IEA). *Net Zero by 2050—A Roadmap for the Global Energy Sector*; International Energy Agency: Paris, France, 2021.
2. Tester, J.W. *The Future of Geothermal Energy: Impact of Enhanced Geothermal Systems (EGS) on the United States in the 21st Century*; Massachusetts Institute of Technology: Cambridge, MA, USA, 2006.
3. United Nations (UN). *Transforming Our World: The 2030 Agenda for Sustainable Development*; United Nations: New York, NY, USA, 2015.
4. Council of the European Union Council Conclusions on Climate and Energy Diplomacy. *Bolstering EU Climate and Energy Diplomacy in a Critical Decade*; European Union: Brussels, Belgium, 2023.
5. Ervine, C. Directive 2004/39/Ec of the European Parliament and of the Council of 21 April 2004. In *Core Statutes on Company Law*; Macmillan Education: London, UK, 2015; pp. 757–759, ISBN 978-1-137-54506-0.
6. U.S. Department of Energy. *GeoVision: Harnessing the Heat Beneath Our Feet*; U.S. Department of Energy: Washington, DC, USA, 2019.
7. Espanya; Ministerio de Industria, Comercio y Turismo; Espanya; Ministerio de Ciencia e Innovación; Instituto para la Diversificación y Ahorro de la Energía; Instituto Geológico y Minero de España. *Manual de Geotermia*; IDAE: Madrid, Spain, 2008; ISBN 978-84-96680-35-7.
8. Instituto para la Diversificación y Ahorro de la Energía (IDAE). *Guía Técnica de Diseño de Sistemas de Intercambio Geotérmico de Circuito Cerrado*; Instituto para la Diversificación y Ahorro de la Energía (IDAE): Madrid, Spain, 2012.
9. Assad, M.E.H.; Bani-Hani, E.; Khalil, M. Performance of geothermal power plants (single, dual, and binary) to compensate for LHC-CERN power consumption: Comparative study. *Geotherm. Energy* **2017**, *5*, 17. [CrossRef]
10. Urresta, E.; Moya, M.; Campana, C.; Cruz, C. Ground Thermal Conductivity Estimation Using the Thermal Response Test with a Horizontal Ground Heat Exchanger. *Geothermics* **2021**, *96*, 102213. [CrossRef]
11. Chomać-Pierzecka, E.; Sobczak, A.; Soboń, D. The Potential and Development of the Geothermal Energy Market in Poland and the Baltic States—Selected Aspects. *Energies* **2022**, *15*, 4142. [CrossRef]
12. Trillo, G.L.; Angulo, V.R. *Guía de La Energía Geotérmica*; Dirección General de Industria, Energía y Minas: Madrid, Spain, 2008.
13. Sañudo-Fontaneda, L.A.; Roces-García, J.; Coupe, S.J.; Barrios-Crespo, E.; Rey-Mahía, C.; Álvarez-Rabanal, F.P.; Lashford, C. Descriptive Analysis of the Performance of a Vegetated Swale through Long-Term Hydrological Monitoring: A Case Study from Coventry, UK. *Water* **2020**, *12*, 2781. [CrossRef]
14. Congedo, P.M.; Colangelo, G.; Starace, G. CFD Simulations of Horizontal Ground Heat Exchangers: A Comparison among Different Configurations. *Appl. Therm. Eng.* **2012**, *33–34*, 24–32. [CrossRef]
15. Di Sipio, E.; Bertermann, D. Factors Influencing the Thermal Efficiency of Horizontal Ground Heat Exchangers. *Energies* **2017**, *10*, 1897. [CrossRef]
16. Rey-Mahia, C.; Álvarez-Rabanal, F.P.; Coupe, S.J.; Sañudo Fontaneda, L.Á. The Role of Geothermal Heat Pump Systems in the Water–Energy Nexus. In *Geothermal Heat Pump Systems; Green Energy and Technology*; Springer International Publishing: Cham, Switzerland, 2023; ISBN 978-3-031-24523-7.
17. De Oliveira, G.C.; Bertone, E.; Stewart, R.A. Challenges, Opportunities, and Strategies for Undertaking Integrated Precinct-Scale Energy–Water System Planning. *Renew. Sustain. Energy Rev.* **2022**, *161*, 112297. [CrossRef]

18. Faraj-Lloyd, A.; Charlesworth, S.M.; Coupe, S.J. Sustainable Drainage Systems and Energy: Generation and Reduction. In *Sustainable Surface Water Management*; Charlesworth, S.M., Booth, C.A., Eds.; Wiley: Hoboken, NJ, USA, 2017; pp. 177–192, ISBN 978-1-118-89770-6.
19. Chan, F.K.S.; Griffiths, J.A.; Higgitt, D.; Xu, S.; Zhu, F.; Tang, Y.-T.; Xu, Y.; Thorne, C.R. "Sponge City" in China—A Breakthrough of Planning and Flood Risk Management in the Urban Context. *Land Use Policy* **2018**, *76*, 772–778. [CrossRef]
20. Ayuntamiento de Madrid. *Guía Básica de Diseño de Sistemas de Gestión Sostenible de Aguas Pluviales En Zonas Verdes y Otros Espacios Libres*; Dirección General de Gestión del Agua y Zonas Verdes: Madrid, Spain, 2018.
21. Fletcher, T.D.; Shuster, W.; Hunt, W.F.; Ashley, R.; Butler, D.; Arthur, S.; Trowsdale, S.; Barraud, S.; Semadeni-Davies, A.; Bertrand-Krajewski, J.-L.; et al. SUDS, LID, BMPs, WSUD and More—The Evolution and Application of Terminology Surrounding Urban Drainage. *Urban Water J.* **2015**, *12*, 525–542. [CrossRef]
22. Sañudo-Fontaneda, L.A.; Rodriguez-Hernandez, J.; Castro-Fresno, D. *Diseño y Construcción de Sistemas Urbanos de Drenaje Sostenible (SUDS)*; School of Civil Engineering of the Universidad de Cantabria: Santander, Spain, 2012.
23. North Carolina Department of Environmental Quality. *Stormwater Design Maintenance*; North Carolina Department of Environmental Quality: Raleigh, NC, USA, 2017.
24. Charlesworth, S.M.; Faraj-Llyod, A.S.; Coupe, S.J. Renewable Energy Combined with Sustainable Drainage: Ground Source Heat and Pervious Paving. *Renew. Sustain. Energy Rev.* **2017**, *68*, 912–919. [CrossRef]
25. Jato-Espino, D.; Sañudo-Fontaneda, L.A.; Andrés-Valeri, V.C. Green Infrastructure: Cost-Effective Nature-Based Solutions for Safeguarding the Environment and Protecting Human Health and Well-Being. In *Handbook of Environmental Materials Management*; Hussain, C.M., Ed.; Springer International Publishing: Cham, Switzerland, 2018; pp. 1–27. ISBN 978-3-319-58538-3.
26. del-Castillo-García, G.; Borinaga-Treviño, R.; Sañudo-Fontaneda, L.A.; Pascual-Muñoz, P. Influence of Pervious Pavement Systems on Heat Dissipation from a Horizontal Geothermal System. *Eur. J. Environ. Civ. Eng.* **2013**, *17*, 956–967. [CrossRef]
27. Tota-Maharaj, K.; Scholz, M.; Ahmed, T.; French, C.; Pagaling, E. The Synergy of Permeable Pavements and Geothermal Heat Pumps for Stormwater Treatment and Reuse. *Environ. Technol.* **2010**, *31*, 1517–1531. [CrossRef]
28. Tota-Maharaj, K.; Paul, P. Sustainable Approaches for Stormwater Quality Improvements with Experimental Geothermal Paving Systems. *Sustainability* **2015**, *7*, 1388–1410. [CrossRef]
29. Rey-Mahía, C.; Sañudo-Fontaneda, L.A.; Andrés-Valeri, V.C.; Álvarez-Rabanal, F.P.; Coupe, S.J.; Roces-García, J. Evaluating the Thermal Performance of Wet Swales Housing Ground Source Heat Pump Elements through Laboratory Modelling. *Sustainability* **2019**, *11*, 3118. [CrossRef]
30. Mayor's Office of Transportatios and Utilities, City of Philadelphia. *City of Philadelphia Green Streets Desing Manual*; Mayor's Office of Transportatios and Utilities, City of Philadelphia: Philadelphia, PA, USA, 2014.
31. Woods-Ballard, B.; Wilson, S.; Udale-Clarke, H.; Illman, S.; Scott, T.; Ashley, R.; Kellagher, R. *The SuDS Manual*; CIRIA: London, UK, 2015; ISBN 978-0-86017-760-9.
32. Florides, G.; Kalogirou, S. Ground Heat Exchangers—A Review of Systems, Models and Applications. *Renew. Energy* **2007**, *32*, 2461–2478. [CrossRef]
33. Aresti, L.; Christodoulides, P.; Florides, G. A Review of the Design Aspects of Ground Heat Exchangers. *Renew. Sustain. Energy Rev.* **2018**, *92*, 757–773. [CrossRef]
34. Gil, A.G. *Geotermia Somera: Fundamentos Teóricos y Aplicación*; Instituto Geológico y Minero de España: Madrid, Spain, 2020; ISBN 978-84-9138-105-1.
35. Hou, G.; Taherian, H.; Song, Y.; Jiang, W.; Chen, D. A Systematic Review on Optimal Analysis of Horizontal Heat Exchangers in Ground Source Heat Pump Systems. *Renew. Sustain. Energy Rev.* **2022**, *154*, 111830. [CrossRef]
36. Rottmann, M.; Beikircher, T.; Ebert, H.-P. Thermal Conductivity of Evacuated Expanded Perlite Measured with Guarded-Hot-Plate and Transient-Hot-Wire Method at Temperatures between 295 K and 1073 K. *Int. J. Therm. Sci.* **2020**, *152*, 106338. [CrossRef]
37. Kim, D.; Oh, S. Measurement and Comparison of Thermal Conductivity of Porous Materials Using Box, Dual-Needle, and Single-Needle Probe Methods-A Case Study. *Int. Commun. Heat Mass Transf.* **2020**, *118*, 104815. [CrossRef]
38. Poulsen, S.E.; Andersen, T.R.; Tordrup, K.W. Full-Scale Demonstration of Combined Ground Source Heating and Sustainable Urban Drainage in Roadbeds. *Energies* **2022**, *15*, 4505. [CrossRef]
39. Andersen, T.R.; Poulsen, S.E.; Tordrup, K.W. The Climate Road—A Multifunctional Full-Scale Demonstration Road That Prevents Flooding and Produces Green Energy. *Water* **2022**, *14*, 666. [CrossRef]
40. Rey-Mahía, C.; Álvarez-Rabanal, F.P.; Sañudo-Fontaneda, L.A.; Hidalgo-Tostado, M.; Menéndez Suárez-Inclán, A. An Experimental and Numerical Approach to Multifunctional Urban Surfaces through Blue Roofs. *Sustainability* **2022**, *14*, 1815. [CrossRef]
41. Borinaga-Treviño, R.; Pascual-Muñoz, P.; Castro-Fresno, D.; Del Coz-Díaz, J.J. Study of Different Grouting Materials Used in Vertical Geothermal Closed-Loop Heat Exchangers. *Appl. Therm. Eng.* **2013**, *50*, 159–167. [CrossRef]
42. Di Sipio, E.; Chiesa, S.; Destro, E.; Galgaro, A.; Giaretta, A.; Gola, G.; Manzella, A. Rock Thermal Conductivity as Key Parameter for Geothermal Numerical Models. *Energy Procedia* **2013**, *40*, 87–94. [CrossRef]
43. Del Coz Díaz, J.J.; Álvarez Rabanal, F.P.; García Nieto, P.J.; Domínguez Hernández, J.; Rodríguez Soria, B.; Pérez-Bella, J.M. Hygrothermal Properties of Lightweight Concrete: Experiments and Numerical Fitting Study. *Constr. Build. Mater.* **2013**, *40*, 543–555. [CrossRef]
44. Fuente-García, L.; Perales-Momparler, S.; Rico-Cortés, M.; Andrés-Doménech, I.; Marco-Segura, J.B. *Guía Básica para el Diseño de Sistemas Urbanos de Drenaje Sostenible en la Ciudad de València*; Ajuntament de València: Valencia, Spain, 2021; ISBN 978-84-9089-386-9.

45. Rashad, A.M. Lightweight Expanded Clay Aggregate as a Building Material—An Overview. *Constr. Build. Mater.* **2018**, *170*, 757–775. [CrossRef]
46. *UNE-EN 13242:2003+A1:2008*; Aggregates for Unbound and Hydraulically Bound Materials for Use in Civil Engineering Work and Road Construction. European Standards: Plzen, Czech Republic, 2008.
47. *UNE-EN 933-1:2012*; Test for Geometrical Properties of Aggregates. Part 1: Determination of Particle Size Distribution. Sieving Method. European Standards: Plzen, Czech Republic, 2012.
48. *UNE-EN ISO 22007-2:2023*; Plastics. Determination of Thermal Conductivity and Thermal Diffusivity. Part 2: Transient Plane Heat Source (Hot Disc) Method. European Standards: Plzen, Czech Republic, 2023.
49. *ASTM D7984:21*; Standard Test Method for Measurement of Thermal Effusivity of Fabrics Using a Modified Transient Plane Source (MTPS) Instrument. ASTM International: West Conshohocken, PA, USA, 2021.
50. *UNE-EN 1097-6:2014*; Tests for Mechanical and Physical Properties of Aggregates—Part 6: Determination of Particle Density and Water Absorption. European Standards: Plzen, Czech Republic, 2014.
51. *UNE-EN ISO 8990:1997*; Thermal Insulation. Determination of Steady-State Thermal Transmission Properties. Calibrated and Guarded Hot Box (ISO 8990:1994). European Standards: Plzen, Czech Republic, 1997.
52. *ASTM C1363:19*; Standard Test Method for Thermal Performance of Building Materials and Envelope Assemblies by Means of a Hot Box Apparatus. ASTM International: West Conshohocken, PA, USA, 2019.
53. Cengel, Y. *Transferencia de Calor y Masa. Fundamentos y Aplicaciones*; McGraw-Hill Education: Columbus, OH, USA, 2020; ISBN 978-607-15-1461-5.
54. Parikh, M.; Shah, S.; Vaghela, H.; Parwani, A.K. A Comprehensive Experimental and Numerical Estimation of Thermal Contact Conductance. *Int. J. Therm. Sci.* **2022**, *172*, 107285. [CrossRef]
55. Barlat, F.; Lian, J. *Element Reference Ansys*; Ansys Inc.: Canonsburg, PA, USA, 2021.
56. *UNE-EN ISO 6946:2021*; Building Components and Building Elements—Thermal Resistance and Thermal Transmittance—Calculation Methods (ISO 6946:2017, Corrected Version 2021-12). European Standards: Plzen, Czech Republic, 2021.
57. Del Coz-Díaz, J.J.; Álvarez-Rabanal, F.P.; Alonso-Martínez, M.; Martínez-Martínez, J.E. Thermal Inertia Characterization of Multilayer Lightweight Walls: Numerical Analysis and Experimental Validation. *Appl. Sci.* **2021**, *11*, 5008. [CrossRef]
58. Antony, J. Design of Experiments for Engineers and Scientists. In *Design of Experiments for Engineers and Scientists*; Elsevier: New York, NY, USA, 2014; pp. i–iii. ISBN 978-0-08-099417-8.
59. Acharya, S.; Saini, T.R.S.; Sundaram, V.; Kumar, H. Selection of Optimal Composition of MR Fluid for a Brake Designed Using MOGA Optimization Coupled with Magnetic FEA Analysis. *J. Intell. Mater. Syst. Struct.* **2021**, *32*, 1831–1854. [CrossRef]
60. Gobierno de España Agencia Estatal de Meteorología—AEMET. Available online: https://aemet.com/ (accessed on 27 August 2023).
61. Sivaprasad, A.; Basu, P. Comparative Assessment of Transient- and Steady-State Soil Thermal Conductivity Using a Specially Designed Consolidometer. *Geothermics* **2023**, *107*, 102583. [CrossRef]